Appendix A
Scattering Rates

In this appendix, the fit functions for the microscopically calculated scattering rates are discussed. Due to the principle of detailed balance, the out-scattering rates may be calculated from the in-scattering rates [1, 2]. The detailed balance relations read in their dimensionless form with respect to time $t' = 2\kappa t$

$$s_b^{\text{out}} = s_b^{\text{in}} e^{-\frac{\Delta E_b}{k_{\text{bo}}\mathcal{T}}} \left[e^{c_b W_b} - 1 \right]^{-1}, \quad \text{for} \quad b \in \{e, h\}, \tag{A.1}$$

where the coefficients $c_b = 2N^{\text{QD}}/(D_b k_{\text{bo}}\mathcal{T})$ were introduced. Here, $D_b = m_b/(\pi\hbar^2)$ are the 2D densities of state in the carrier reservoir with the effective masses m_b. The temperature is denoted by $\mathcal{T}$, and k_{bo} is Boltzmann's constant. Further, $\Delta E_e \equiv E_e^{\text{QW}} - E_e^{\text{QD}}$ and $\Delta E_h \equiv E_h^{\text{QD}} - E_h^{\text{QW}}$ are the energy differences between the QD levels E_e^{QD} and E_h^{QD} and the band edges of the QW E_e^{QW} and E_h^{QW} for electrons and holes, respectively, (see Fig. A.1).

In this work, three different sets of microscopically calculated band structures are considered named reference, slow, and fast. They differ in the energy spacings ΔE_e and ΔE_h between QD levels and the band edge of the carrier reservoir (see Table 2.1), which results in different carrier lifetimes $t_b^{-1} = (s_b^{\text{in}} + s_b^{\text{out}})$ as discussed in Sect. 2.2.

A.1 Fit Functions for Scattering Rates

For all three sets of scattering rates, the same functional dependence of s_b^{in} on the reservoir populations are assumed. They are fitted by forth order polynomials in W_e and W_h multiplied by a tanh, which allows for a good agreement with the microscopically calculated rates at low values of the reservoir populations W_e and W_h. The fit functions read

C. Otto, *Dynamics of Quantum Dot Lasers*,
Springer Theses, DOI: 10.1007/978-3-319-03786-8,

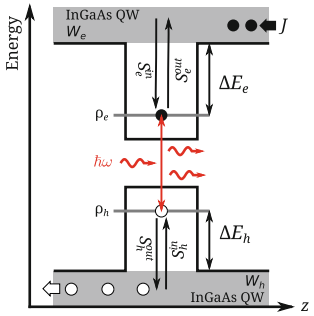

Fig. A.1 Energy diagram of the band structure across a QD. The ground state lasing energy is labeled by $\hbar\omega$. The energetic distances of the QD levels from the band edge of the carrier reservoir (QW) for electrons and holes are marked by ΔE_e and ΔE_h, respectively. The Auger in- and out-scattering rates between QD levels and QW are denoted by $S^{\text{in}}_{e/h}$ and $S^{\text{out}}_{e/h}$, respectively. The occupation probabilities of the QDs are denoted by $\rho_{e/h}$, the reservoir carrier densities are labeled by $W_{e/h}$, and J is the pump current density

Table A.1 Fit parameters for the reference set of carrier scattering rates of Table 2.1 for the QD laser model

Coefficient	Value	Coefficient	Value
a_e	-1.836×10^{-5}	a_h	3.326×10^{-5}
b_e	-7.89×10^{-6}	b_h	-8.064×10^{-4}
$c_{e,1}$	-298187.0	$c_{h,1}$	-6886.56
$c_{e,2}$	38443.3	$c_{h,2}$	-7191.73
$c_{e,3}$	-3287.08	$c_{h,3}$	1117.15
$c_{e,4}$	112.303	$c_{h,4}$	-43.6502
$d_{e,1}$	53262.5	$d_{h,1}$	-17291.4
$d_{e,2}$	571.696	$d_{h,2}$	-13288.4
$d_{e,3}$	-72.5439	$d_{h,3}$	1000.69
$d_{e,4}$	0.683815	$d_{h,4}$	-52.8802

$$s_e^{\text{in}}(W_e, W_h) = \tanh(a_e W_e + b_e) \sum_{i=1}^{4} \left(c_{e,i} W_e^i + d_{e,i} W_h^i\right), \tag{A.2}$$

$$s_h^{\text{in}}(W_e, W_h) = \tanh(a_h W_h + b_h) \sum_{i=1}^{4} \left(c_{h,i} W_e^i + d_{h,i} W_h^i\right), \tag{A.3}$$

where the coefficients $a_{e/h}$, $b_{e/h}$, $c_{e/h,i}$, and d_{e/h_i} for $i \in \{1, 2, 3, 4\}$ are listed in Tables A.1, A.3, and A.5 for reference, slow, and fast setsof scattering rates,

Table A.2 Parameters and steady state values of the solitary QD laser with the fast set of carrier scattering rates

Parameters	Value	Meaning
ΔE_e (ΔE_h)	210 (50) meV	Energy separation QW band edges—QD levels
c_e	4.3070×10^{-1}	Constant for el. out-scattering rate
c_h	4.1155×10^{-2}	Constant for hole out-scattering rate
J/J_{th}	1.50 (3.5)	Ratio of current to current at lasing threshold
J_{th}	3.04	Current at lasing threshold
N_{ph}^0	9074.34 (54244.4)	Steady state photon density
W_e	1.33 (2.09)	Steady state electron density in QW
W_h	1.89 (2.52)	Steady state hole density in QW
ρ_e	0.91 (0.84)	Steady state electron population
ρ_h	0.35 (0.42)	Steady state hole population
s_e^{in}	7.58 (16.10)	Steady state of electron in-scattering rates
s_h^{in}	69.42 (108.79)	Steady state of hole in-scattering rates
s_e^{out}	2.9×10^{-3} (3.2×10^{-3})	Steady state electron out-scattering rates
s_h^{out}	124.25 (143.94)	Steady state hole out-scattering rates
t_e	1.3×10^{-1} (6.2×10^{-2})	Electron lifetime
t_h	5.2×10^{-3} (4.0×10^{-3})	Hole lifetime

Other parameters as in Table 2.2

Table A.3 Fit parameters for the slow set of carrier scattering rates of Table 2.3 for the QD laser model

Coefficient	Value	Coefficient	Value
a_e	-2.6612×10^{-5}	a_h	1.94259×10^{-5}
b_e	-1.64753×10^{-6}	b_h	4.74478×10^{-4}
$c_{e,1}$	−363381.0	$c_{h,1}$	−3601.34
$c_{e,2}$	50519.5	$c_{h,2}$	−15193.1
$c_{e,3}$	−4290.71	$c_{h,3}$	1441.14
$c_{e,4}$	146.177	$c_{h,4}$	−47.7236
$d_{e,1}$	69984.1	$d_{h,1}$	−19129.2
$d_{e,2}$	−74.2397	$d_{h,2}$	−5584.61
$d_{e,3}$	−86.6277	$d_{h,3}$	435.245
$d_{e,4}$	1.65736	$d_{h,4}$	−27.6885

respectively. Further, Tables A.2, A.4, and A.6 list the parameter values for $\Delta E_{e/h}$ and $c_{e/h}$ as well as the steady state values of the dynamical variables, the scattering rates and the dimensionless carrier lifetimes for a pump level of $J = 1.5\, J_{\text{th}}$ and a pump level of $J = 3.5\, J_{\text{th}}$ for reference, slow, and fast sets of scattering rates, respectively.

Table A.4 Parameters and steady state values of the solitary QD laser with the slow set of carrier scattering rates

Parameters	Value	Meaning
ΔE_e (ΔE_h)	140 (120) meV	Energy separation QW band edges – QD levels
c_e	4.3070×10^{-1}	Constant for el. out-scattering rate
c_h	4.1155×10^{-2}	Constant for hole out-scattering rate
J/J_{th}	1.50 (3.5)	Ratio of current to current at lasing threshold
J_{th}	0.576	Current at lasing threshold
N_{ph}^0	6091.92 (27657.3)	Steady state photon density
W_e	0.334 (0.555)	Steady state electron density in QW
W_h	0.438 (0.606)	Steady state hole density in QW
ρ_e	0.684 (0.658)	Steady state electron population
ρ_h	0.580 (0.607)	Steady state hole population
s_e^{in}	2.16 (4.52)	Steady state of electron in-scattering rates
s_h^{in}	5.71 (9.25)	Steady state of hole in-scattering rates
s_e^{out}	6.21×10^{-2} (7.44×10^{-2})	Steady state electron out-scattering rates
s_h^{out}	3.03 (3.53)	Steady state hole out-scattering rates
t_e	4.50×10^{-1} (2.18×10^{-1})	Electron lifetime
t_h	1.15×10^{-1} (7.82×10^{-2})	Hole lifetime

Other parameters as in Table 2.2

Table A.5 Fit parameters for the fast set of carrier scattering rates of Table 2.1 for the QD laser model

Coefficient	Value	Coefficient	Value
a_e	-1.18454×10^{-5}	a_h	0.542381
b_e	-1.12055×10^{-5}	b_h	−7.51954
$c_{e,1}$	-1.67918×10^{-5}	$c_{h,1}$	6.93691
$c_{e,2}$	246065	$c_{h,2}$	−3.05438
$c_{e,3}$	−20090.5	$c_{h,3}$	0.436126
$c_{e,4}$	666.063	$c_{h,4}$	−0.021217
$d_{e,1}$	305994	$d_{h,1}$	−10.1779
$d_{e,2}$	1224.67	$d_{h,2}$	−2.57347
$d_{e,3}$	−758.135	$d_{h,3}$	0.159026
$d_{e,4}$	21.2669	$d_{h,4}$	−0.00408522

Table A.6 Parameters and steady state values of the solitary QD laser with the fast set of carrier scattering rates

Parameters	Value	Meaning
ΔE_e (ΔE_h)	74 (40) meV	Energy separation QW band edges—QD levels
c_e	4.3070×10^{-1}	Constant for el. out-scattering rate
c_h	4.1155×10^{-2}	Constant for hole out-scattering rate
J/J_{th}	1.50 (3.5)	Ratio of current to current at lasing threshold
J_{th}	6.78947	Current at lasing threshold
N_{ph}^0	39532.1 (191311)	Steady state photon density
W_e	2.040 (2.946)	Steady state el. for $k = 0$
W_h	2.639 (3.486)	Steady state hole density for $k = 0$
ρ_e	0.932 (0.903)	Steady state electron population
ρ_h	0.333 (0.362)	Steady state hole population
s_e^{in}	62.15 (102.43)	Steady state of electron in-scattering rates
s_h^{in}	37.28 (57.14)	Steady state of hole in-scattering rates
s_e^{out}	2.52 (2.29)	Steady state electron out-scattering rates
s_h^{out}	69.16 (78.83)	Steady state hole out-scattering rates
t_e	1.55×10^{-2} (9.55×10^{-2})	Electron lifetime
t_h	9.39×10^{-3} (7.35×10^{-3})	Hole lifetime

Other parameters as in Table 2.2

Appendix B
Resolving the Singularity at $\gamma \to 0$

In this appendix, it is discussed how the singularity of the dynamical Eqs. (2.4) for $\gamma \to 0$ can be resolved by rescaling the dimensionless time t' as well as the dynamical variables N_{ph}, ρ_e, ρ_h, W_e, and W_h. The initial set of ordinary differential equations reads

$$N'_{\mathrm{ph}} = \Big[g(\rho_e + \rho_h - 1) - 1\Big] N_{\mathrm{ph}}, \tag{B.1a}$$

$$\rho'_e = \gamma\Big[s_e^{\mathrm{in}}(1-\rho_e) - s_e^{\mathrm{out}}\rho_e - r_w(\rho_e + \rho_h - 1)N_{\mathrm{ph}} - \rho_e\rho_h\Big], \tag{B.1b}$$

$$\rho'_h = \gamma\Big[s_h^{\mathrm{in}}(1-\rho_h) - s_h^{\mathrm{out}}\rho_h - r_w(\rho_e + \rho_h - 1)N_{\mathrm{ph}} - \rho_e\rho_h\Big], \tag{B.1c}$$

$$W'_e = \gamma\Big[J - s_e^{\mathrm{in}}(1-\rho_e) + s_e^{\mathrm{out}}\rho_e - cW_eW_h\Big], \tag{B.1d}$$

$$W'_h = \gamma\Big[J - s_h^{\mathrm{in}}(1-\rho_h) + s_h^{\mathrm{out}}\rho_h - cW_eW_h\Big], \tag{B.1e}$$

where the spontaneous emission in Eq. (B.1) has been neglected ($d = 0$). First note that the limit $\gamma \to 0$ is indeed singular. Singular means that $\gamma = 0$ leads to a qualitatively different solution than finite $\gamma \ll 1$ [3, 4]. Setting $\gamma = 0$, yields $\rho'_e = \rho'_h = W'_e = W'_h = 0$, which results in constant carrier populations and thus in an exponential increase or decrease of N_{ph}. In contrast, for finite γ, stable steady state lasing is observed in the numerical simulations. Perturbations from this equilibrium decay either exponentially in the overdamped limit of the set of fast scattering rates or for small values of γ, damped ROs are observed for the slow, reference, and very fast rates (cf. Fig. 2.5). Thus, for γ small, we would expect that the leading order problem in γ is conservative and the damping is introduced by the higher order contributions [5]. Therefore, we try to find a coordinate transformation that resolves the singularity at $\gamma = 0$. Generally, singular perturbation problems are difficult to solve, because no systematic technique exists. For the present problem, the singularity can be removed by a change of variables that is known from rate equations of conventional semiconductor QW lasers [6]. The key observation is that the frequency of the ROs scales like $\sqrt{\gamma}$. Rescaling time with respect to the time

C. Otto, *Dynamics of Quantum Dot Lasers*,
Springer Theses, DOI: 10.1007/978-3-319-03786-8,

scale of the ROs permits to resolve the singularity [5]. The scalings of the deviations from the steady states of the carrier variables are then obtained by balancing the dynamical equations.

At first, deviations (y, u_e, u_e, v_e, v_h) from the lasing steady state $(N_{\mathrm{ph}}^0, \rho_e^0, \rho_h^0, W_e^0, W_h^0)$ and a new time s are introduced by

$$y \equiv \frac{N_{\mathrm{ph}} - N_{\mathrm{ph}}^0}{a_{\mathrm{ph}}}, \quad u_b \equiv \frac{\rho_b - \rho_b^0}{a_b}, \quad v_b \equiv \frac{W_b - W_b^0}{b_b}, \quad \text{and} \quad s \equiv \eta t', \tag{B.2}$$

where $b = e$ and $b = h$ denote electrons and holes, respectively. The coefficients a_{ph}, a_b, v_b, and η are functions of γ, and their scalings have to be determined in the following. Inserting the ansatz (B.2) into Eq. (B.1), yields

$$\dot{y} = \frac{1}{\eta}\left[\left(\frac{N_{\mathrm{ph}}^0}{a_{\mathrm{ph}}} + y\right) g(a_e u_e + a_h u_h)\right], \tag{B.3a}$$

$$\dot{u}_e = -\frac{\gamma}{\eta a_e}\left[\begin{array}{c} a_e t_e^{-1} u_e + a_{\mathrm{ph}} y r_w (\rho_e^0 + \rho_h^0 - 1 + a_e u_e + a_h u_h) \\ + r_w N_{\mathrm{ph}}^0 (a_e u_e + a_h u_h) + a_e u_e \rho_h^0 + a_h u_h \rho_e^0 + a_e a_h u_e u_h \end{array}\right], \tag{B.3b}$$

$$\dot{u}_h = -\frac{\gamma}{\eta a_h}\left[\begin{array}{c} a_h t_h^{-1} u_h + a_{\mathrm{ph}} y r_w (\rho_e^0 + \rho_h^0 - 1 + a_e u_e + a_h u_h) \\ + r_w N_{\mathrm{ph}}^0 (a_e u_e + a_h u_h) + a_e u_e \rho_h^0 + a_h u_h \rho_e^0 + a_e a_h u_e u_h \end{array}\right], \tag{B.3c}$$

$$\dot{v}_e = \frac{\gamma}{\eta b_e}\left[a_e t_e^{-1} u_e - c(b_h v_h W_e^0 + b_e v_e W_h^0 + b_e b_h v_e v_h)\right], \tag{B.3d}$$

$$\dot{v}_h = \frac{\gamma}{\eta b_h}\left[a_h t_h^{-1} u_h - c(b_h v_h W_e^0 + b_e v_e W_h^0 + b_e b_h v_e v_h)\right], \tag{B.3e}$$

where the gain-clamping relation (2.25) was used to simplify the photon equation (B.3a), and $t_b^{-1} \equiv s_e^{\mathrm{in}} + s_e^{\mathrm{out}}$ was introduced. Furthermore, the carrier Eqs. B.3b–B.3e have been simplified by using steady state relations, which were obtained by equating to zero the right hand sides of Eqs. (B.1b)–(B.1e).

In a next step, scaling laws for the coefficients are derived under the conditions that in the rescaled quations [7]

(i) The time scale separation γ does not multiply the complete right hand sides of the carrier equations (B.3b)–(B.3e) to resolve the singularity at $\gamma = 0$.
(ii) The number of independent parameters is reduced by regrouping them into dimensionless groups.

To balance the photon equation (B.3a), a_e and a_h have to scale like η, because the derivative of y with respect to the slow time s is assumed to be of order $\mathcal{O}(1)$. Thus, the choice $a_e = \mathcal{O}(\eta)$ and $a_h = \mathcal{O}(\eta)$ permits to balance all the terms on the right hand side of the equation if we additionally assume the $a_{\mathrm{ph}} = \mathcal{O}(N_{\mathrm{ph}}^0)$. The concept to balance as many terms as possible is known as principle of dominant balance [4]. As mentioned above, the corresponding transformation for conventional class B semiconductor lasers [6] suggests that $\eta = \mathcal{O}(\sqrt{\gamma})$. This choice additionally prevents that γ multiplies the full right hand sides of Eqs. (B.3b) and (B.3c). A simple choice

to reduce the number of the independent parameters is to set equal a_e and a_h, i.e., to introduce $a \equiv a_e = a_h$. Moreover, the photon equation (B.3a) may be simplified by choosing $a_{\mathrm{ph}} = N_{\mathrm{ph}}^0$ and setting the dimensionless group ga/η equal to unity, which yields

$$\frac{ga}{\eta} = 1 \quad \Leftrightarrow \quad a = g^{-1}\eta = g^{-1}\sqrt{\gamma}\omega, \tag{B.4}$$

where $\eta = \sqrt{\gamma}\omega$ with $\omega = \mathcal{O}(1)$ has been used in the last equality. Inserting these scaling laws into the dynamical equations (B.2), they simplify as

$$\dot{y} = (u_e + u_h)\,(1 + y)\,, \tag{B.5a}$$

$$\omega^2 \dot{u}_e = -r_w N_{\mathrm{ph}}^0 y - \left[\begin{array}{c} \sqrt{\gamma}\omega\left(t_e^{-1}u_e + r_w N_{\mathrm{ph}}^0(u_e + u_h)(1 + y) + u_e\rho_h^0 + u_h\rho_e^0\right) \\ +\gamma g^{-1}\omega^2 u_e u_h \end{array}\right], \tag{B.5b}$$

$$\omega^2 \dot{u}_h = -r_w N_{\mathrm{ph}}^0 y - \left[\begin{array}{c} \sqrt{\gamma}\omega\left(t_h^{-1}u_h + r_w N_{\mathrm{ph}}^0(u_e + u_h)(1 + y) + u_e\rho_h^0 + u_h\rho_e^0\right) \\ +\gamma g^{-1}\omega^2 u_e u_h \end{array}\right], \tag{B.5c}$$

$$\omega\dot{v}_e = \frac{\sqrt{\gamma}}{b_e}\left[\sqrt{\gamma}g^{-1}\omega t_e^{-1}u_e - c(b_h v_h W_e^0 + b_e v_e W_h^0 + b_e b_h v_e v_h)\right], \tag{B.5d}$$

$$\omega\dot{v}_h = \frac{\sqrt{\gamma}}{b_h}\left[\sqrt{\gamma}g^{-1}\omega t_h^{-1}u_h - c(b_h v_h W_e^0 + b_e v_e W_h^0 + b_e b_h v_e v_h)\right], \tag{B.5e}$$

where the gain-clamping relation (2.25) was employed to simplify Eqs. (B.5b) and (B.5c). In Sect. 2.2, it was discussed that the scattering rates have a crucial impact on the damping of the ROs, which in terms influences the tolerance of the laser subject to optical injection and optical feedback. Therefore, the coefficients b_e and b_h in Eqs. (B.5d) and (B.5e) are chosen such that the first terms in the brackets on the right hand sides of the equations, which are proportional to the carrier lifetimes t_e and t_h, constitute the leading order terms of these equations. A simple choice for b_e and b_h that simplifies the leading order problem is $b \equiv b_e = b_h = g^{-1}\gamma\omega$. Inserting b into Eqs. (B.5d) and (B.5e), yields the final set of equations

$$\dot{y} = (u_e + u_h)\,(1 + y)\,, \tag{B.6a}$$

$$\omega^2 \dot{u}_e = -r_w N_{\mathrm{ph}}^0 y - \left[\begin{array}{c} \sqrt{\gamma}\omega \left(t_e^{-1} u_e + r_w N_{\mathrm{ph}}^0 (u_e + u_h)(1 + y) + u_e \rho_h^0 + u_h \rho_e^0 \right) \\ + \gamma g^{-1} \omega^2 u_e u_h \end{array} \right], \tag{B.6b}$$

$$\omega^2 \dot{u}_h = -r_w N_{\mathrm{ph}}^0 y - \left[\begin{array}{c} \sqrt{\gamma}\omega \left(t_h^{-1} u_h + r_w N_{\mathrm{ph}}^0 (u_e + u_h)(1 + y) + u_e \rho_h^0 + u_h \rho_e^0 \right) \\ + \gamma g^{-1} \omega^2 u_e u_h \end{array} \right], \tag{B.6c}$$

$$\omega \dot{v}_e = t_e^{-1} u_e - c\sqrt{\gamma}(v_h W_e^0 + v_e W_h^0) + c\gamma^{3/2} g^{-1} \omega v_e v_h, \tag{B.6d}$$

$$\omega \dot{v}_h = t_h^{-1} u_h - c\sqrt{\gamma}(v_h W_e^0 + v_e W_h^0) + c\gamma^{3/2} g^{-1} \omega v_e v_h. \tag{B.6e}$$

Appendix C
Loci of Hopf Bifurcations in (C,K)-Plane

In this appendix, the loci of the Hopf bifurcation lines for the single mode laser subject to feedback in the plane spanned by the feedback phase C and the feedback strength K are derived. From Eq. 4.53, we obtain

$$\delta\omega^{\mathrm{s}}\tau = \arctan(\alpha) - C \pm \arccos\Big(-\frac{\mathcal{G}}{\tilde{k}_{\mathrm{eff}}^{H}}\Big) + 2n\pi, \tag{C.1}$$

Further, rewriting the transcendental Eq. 4.7 in the same way, yields

$$\delta\omega^{\mathrm{s}}\tau = -\tilde{k}_{\mathrm{eff}}^{H}\sin\big(C + \delta\omega^{\mathrm{s}}\tau + \arctan(\alpha)\big). \tag{C.2}$$

Inserting Eq. (C.1) into Eq. (C.2) permits to eliminate $\delta\omega^{\mathrm{s}}\tau$

$$\begin{aligned} C =& \arctan(\alpha) \pm \arccos\Big(-\frac{\mathcal{G}}{\tilde{k}_{\mathrm{eff}}^{H}}\Big) \\ &+ \tilde{k}_{\mathrm{eff}}^{H}\sin\Big(2\arctan(\alpha) \pm \arccos\Big(-\frac{\mathcal{G}}{\tilde{k}_{\mathrm{eff}}^{H}}\Big)\Big) + 2n\pi. \end{aligned} \tag{C.3}$$

With the help of some trigonometric identities[1] Eq. (C.3) can be expanded as

[1] In order to simplify Eq. (C.3), several trigonometric identities are employed for resolving the sine

$$\sin(x \pm y) = \sin(x)\cos(y) \pm \sin(y)\cos(x), \tag{C.4}$$

$$\cos(x \pm y) = \cos(x)\cos(y) \mp \sin(y)\sin(x), \tag{C.5}$$

$$\sin\big(\arctan(x)\big) = \frac{x}{\sqrt{1+x^2}}, \tag{C.6}$$

$$\cos\big(\arctan(x)\big) = \frac{1}{\sqrt{1+x^2}}, \tag{C.7}$$

$$\sin\big(\arccos(x)\big) = \sqrt{1-x^2}., \tag{C.8}$$

C. Otto, *Dynamics of Quantum Dot Lasers*,
Springer Theses, DOI: 10.1007/978-3-319-03786-8,

$$\sin\Big(2\arctan(\alpha) \pm \arccos\Big(-\frac{\mathcal{G}}{\tilde{k}^H_{\text{eff}}}\Big)\Big) \overset{(C.4)}{=} \sin\Big(2\arctan(\alpha)\Big)\cos\Big(\arccos\Big(-\frac{\mathcal{G}}{\tilde{k}^H_{\text{eff}}}\Big)\Big) \pm \cos\Big(2\arctan(\alpha)\Big)\sin\Big(\arccos\Big(-\frac{\mathcal{G}}{\tilde{k}^H_{\text{eff}}}\Big)\Big).$$

Using

$$\sin\Big(2\arctan(\alpha)\Big) \overset{(C.4)}{=} 2\sin\Big(\arctan(\alpha)\Big)\cos\Big(\arctan(\alpha)\Big) \overset{(C.6),(C.7)}{=} \frac{2\alpha}{1+\alpha^2}$$

and

$$\cos\Big(2\arctan(\alpha)\Big) \overset{(C.5)}{=} \cos^2\Big(\arctan(\alpha)\Big) - \sin^2\Big(\arctan(\alpha)\Big) \overset{(C.6),(C.7)}{=} \frac{1-\alpha^2}{1+\alpha^2},$$

one obtains

$$\begin{aligned}
&\sin\Big(2\arctan(\alpha) \pm \arccos\Big(-\frac{\mathcal{G}}{\tilde{k}^H_{\text{eff}}}\Big)\Big) \\
&= -\frac{2\alpha\mathcal{G}}{\tilde{k}^H_{\text{eff}}(1+\alpha^2)} \pm \frac{1-\alpha^2}{1+\alpha^2}\sin\Big(\arccos\Big(-\frac{\mathcal{G}}{\tilde{k}^H_{\text{eff}}}\Big)\Big) \\
&\overset{(C.8)}{=} -\frac{2\alpha\mathcal{G}}{\tilde{k}^H_{\text{eff}}(1+\alpha^2)} \pm \frac{1-\alpha^2}{1+\alpha^2}\sqrt{1-\frac{\mathcal{G}^2}{(\tilde{k}^H_{\text{eff}})^2}} = \frac{1}{\tilde{k}^H_{\text{eff}}}\Big\{-\frac{2\alpha\mathcal{G}}{1+\alpha^2} \pm \frac{1-\alpha^2}{1+\alpha^2}\sqrt{(\tilde{k}^H_{\text{eff}})^2-\mathcal{G}^2}\Big\}.
\end{aligned}$$

Inserting this result into Eq. (C.3), yields the final expression for the loci of Hopf-bifurcations in the $(C,\tilde{k})$-plane [8]

$$C^H_n(k) = \arctan(\alpha) \pm \arccos\Big(\frac{-\mathcal{G}}{\tilde{k}^H_{\text{eff}}}\Big) - \frac{2\alpha\mathcal{G}}{1+\alpha^2} \pm \frac{1-\alpha^2}{1+\alpha^2}\sqrt{(\tilde{k}^H_{\text{eff}})^2-\mathcal{G}^2} + 2n\pi. \tag{C.9}$$

Appendix D
Stochastic Methods

In this appendix, the basic mathematical methods to characterize stochastic processes are discussed.

D.1 Time Average Versus Ensemble Average

A stochastic process $x(t)$ is given by a random variable, which is a function of time, and is thus only statistically characterized. A single event $x(t_1)$ at the time point t_1 only gives us one of the possible state of the system, which in general depends on t_1 and on the realization of the stochastic process, i.e., on its sample path. Therefore, only averaged quantities can be discussed. There are two different averaging procedures: on the one hand, an average can be performed over an ensemble $\{x^{(1)}(t_1), x^{(2)}(t_1), \ldots, x^{(N)}(t_1)\}$ of $N \in \mathbb{N}$ realizations of the stochastic process at a fixed point in time t_1, which is called *ensemble average*. On the other hand, one single realization $x^{(n)}(t)$ of the stochastic process can be averaged over a certain time interval, which is called *time average*. Both averaging procedures are illustrated in Fig. D.1. The graph of a single realization $x^{(n)}(t)$ as a function of time is called a sample path of the stochastic process.

The first order time-average of a stochastic process is defined by

$$\overline{x^{(n)}} \equiv \lim_{T_\mathrm{i}\nearrow\infty} \frac{1}{T_\mathrm{i}} \int_0^{T_\mathrm{i}} x^{(n)}(t')dt', \tag{D.1}$$

where the integration time is denoted by T_i. Further, the correlations of the stochastic process at different time points are described by its autocorrelation function [9–12]

$$\Psi_x(s) \equiv \lim_{T_\mathrm{i}\nearrow\infty} \frac{1}{T_\mathrm{i}} \int_0^{T_\mathrm{i}} x^{(n)}(t')x^{(n)}(t'+s)dt'. \tag{D.2}$$

C. Otto, *Dynamics of Quantum Dot Lasers*,
Springer Theses, DOI: 10.1007/978-3-319-03786-8,

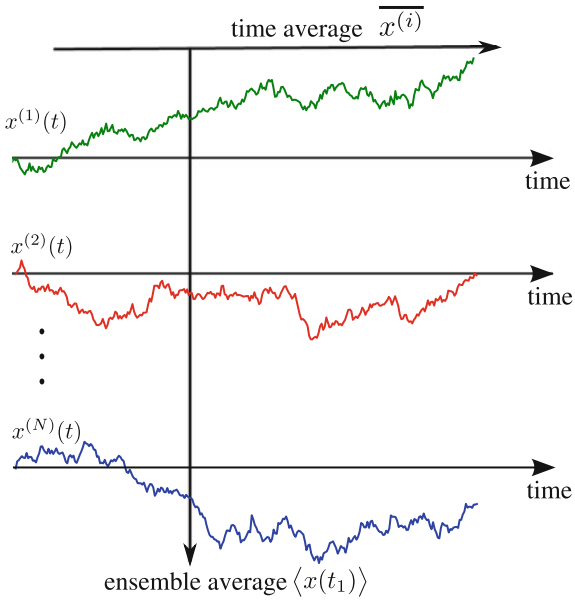

Fig. D.1 Illustration of time and ensemble average. The different sample paths are denoted by $x^{(i)}(t)$ for $i \in \{1, \ldots, N\}$. The time average $\overline{x^{(i)}}$ is performed over one sample path i, while the ensemble average $\langle x(t_1)\rangle$ is performed over the whole ensemble of sample path at a fixed point in time t_1

The first order ensemble average at a time point t_1 is defined by

$$\langle x(t_1)\rangle \equiv \lim_{N\nearrow\infty} \sum_{i=1}^{N} x^{(n)}(t_1) = \int_{\mathbb{R}} x_1 \rho_1(x_1, t_1) dx_1, \tag{D.3}$$

where $\rho_1(x_1, t_1)$ is the probability density of the stochastic process. The correlation of the stochastic process at two different time points t_1 and t_2 averaged over an ensemble of realizations is given by its covariance

$$\langle x(t_1)x(t_2)\rangle \equiv \lim_{N\nearrow\infty} \sum_{i=1}^{N} x^{(n)}(t_1)x^{(n)}(t_2) = \int_{\mathbb{R}} x_1 x_2 \rho_2(x_2, t_2; x_1, t_1) dx_1 dx_2, \tag{D.4}$$

where we have introduced $x_1 \equiv x(t_1)$ and $x_2 \equiv x(t_2)$ as well as the first order probability density function $\rho_1(x_1, t_1)$ and the second order joint probability density function $\rho_2(x_2, t_2; x_1, t_1)$.[2] The ensemble average is thus given by the first moment of the probability function ρ_1, and the second moment reads

$$\langle x^2(t_1)\rangle \equiv \int_{\mathbb{R}} x_1^2 \rho_1(x_1, t_1) dx_1. \tag{D.5}$$

[2] The probability that x is found in the interval $[x_1, x_1 + dx_1]$ is given by $\rho_1(x_1, t_1)dx_1$, and the probability that x is found in $[x_1, x_1 + dx_1]$ at t_1 and in $[x_2, x_2 + dx_2]$ at a (different) time point t_2 is given by $\rho_2(x_2, t_2; x_1, t_1)dx_1 dx_2$

The ensemble average is a convenient concept for the theoretical treatment of a physical systems, since it is directly related to the systems probability density function, which can be generally obtained from the theoretical analysis of the system. However, from an experimental point of view, time-averaging is the more natural procedure since one cannot experimentally prepare an infinite number of identical systems. In the next subsection, we will address the question, under which conditions both averaging procedures are equivalent.

D.2 Statistically Stationary Versus Non-stationary Random Processes

A process is called ergodic in the mean if its time-average (D.1) equals its ensemble average (D.3). Since the time-average (D.1) does not depend on the time point t_1, also the ensemble average has to be stationary (time-independent). Further, a process is called ergodic in the autocorrelation if additionally its autocorrelation function (D.2) equals its covariance (D.4), which implies that the covariance depends only on the time differences $s \equiv t_2 - t_1$ of the considered time points t_1 and t_2, and the second moment (D.5) is independent of time, i.e., stationary.

Processes with constant ensemble average and a covariance that depends only on time differences s are called weakly stationary or wide-sense stationary. From the above considerations, we see that a process, which is ergodic in the autocorrelation is also wide-sense stationary, thus ergodicity implies stationarity, but the inverse is not true [10]. Since the time averaged quantities are obtained by averaging only over one sample function, for an ergodic (and thus a wide-sense stationary) process one sample function is sufficient to obtain all statistical information about the process. For non-stationary processes, the limes $T_\mathrm{i} \nearrow \infty$ does not exist, which means that its time average and its autocorrelation function depend on the integration time T_i. In practice, this is not a disadvantage, because experimental measurements are always carried out for a finite time. The concept of the ensemble average can be employed as before under the assumption that all member functions of the ensemble, i.e., all sample paths have the same probability density function.

D.3 Power Spectral Density and Wiener-Khinchin Theorem

In this section, we will discuss the power spectral density (PSD) or power spectrum, which reveals the frequency content of a stochastic process and is therefore the most universal tool to characterize the typical time scales of the process. Further, the Wiener-Khinchin theorem will be discussed, which states that PSD and autocorrelation function (D.2) of a wide-sense stationary process form a Fourier-pair.

First, we have to introduce the Fourier transform of a stochastic process. Here, we run into the problem that stationary stochastic processes are not integrable, i.e., their $\mathbb{L}^1$-norm $\|\cdot\|_1$ is not finite. This means that they do not belong to the Banach space

$$\mathbb{L}^1 \equiv \left\{ f : \mathbb{R} \longrightarrow \mathbb{C}, \text{ with } \|f\|_1 \equiv \int_{\mathbb{R}} |f(x)| dx < \infty \right\}$$

of measurable functions f. However, every real measurement always has a finite integration time T_i, therefore the Fourier transform can be defined on the Banach space of the gated stochastic processes x_{T_i} [13], defined by

$$x_{T_\mathrm{i}}(t) \equiv \begin{cases} x(t) & \text{for } t \leq T_\mathrm{i}, \\ 0 & \text{else.} \end{cases}$$

The Fourier transform $\mathcal{F}$ and its inverse $\mathcal{F}^{-1}$ of a stochastic process $x_{T_\mathrm{i}}(t)$ is then simply defined by the Fourier transforms of its realizations $x_{T_\mathrm{i}}^{(n)}$ for $n \in \{1, \ldots, N\}$ and $N \in \mathbb{N}$

$$\hat{x}_{T_\mathrm{i}}^{(n)}(\omega) \equiv \mathcal{F}[x_{T_\mathrm{i}}^{(n)}](\omega) \equiv \int_{\mathbb{R}} x_{T_\mathrm{i}}^{(n)}(t) e^{-i\omega t} dt, \tag{D.6a}$$

$$x_{T_\mathrm{i}}^{(n)}(t) = \mathcal{F}^{-1}[\hat{x}_{T_\mathrm{i}}^{(n)}](t) \equiv \frac{1}{2\pi} \int_{\mathbb{R}} \hat{x}_{T_\mathrm{i}}^{(n)}(\omega) e^{i\omega t} d\omega, \tag{D.6b}$$

where $\hat{x}_{T_\mathrm{i}}^{(n)}$ denotes the Fourier transform of the realization $x_{T_\mathrm{i}}^{(n)}$.

With the help of the time-shift property of the Fourier transform $\mathcal{F}[x(t+s)] = \hat{x}(\omega) e^{i\omega s}$, the following relation is obtained

$$\int_{\mathbb{R}} x_{T_\mathrm{i}}^{(n)}(t+s) \left(x_{T_\mathrm{i}}^{(n)}\right)^*(t) dt = \frac{1}{2\pi} \int_{\mathbb{R}} \left|\hat{x}_{T_\mathrm{i}}^{(n)}(\omega)\right|^2 e^{i\omega s} d\omega, \tag{D.7}$$

where $(\cdot)^*$ denotes the complex conjugate. Taking for $s = 0$, the norm of both sides of Eq. (D.7) yields the Plancherel theorem [14]

$$\int_{\mathbb{R}} \left|x_{T_\mathrm{i}}^{(n)}\right|^2 dt = \frac{1}{2\pi} \int_{\mathbb{R}} \left|\hat{x}_{T_\mathrm{i}}^{(n)}(\omega)\right| d\omega. \tag{D.8}$$

It has the physical interpretation that the energy of a signal is the same for the signal itself and for the Fourier transform of the signal, which is sometimes denoted as energy theorem. This means that $|\hat{x}^{(n)}(\omega)|^2$ is the energy density of the harmonic component $e^{i\omega t}$ in units of energy per Hz. For a real non-stationary process x_{T_i}, the energy of the signal will depend on the realization n of the stochastic process. Therefore, to define the time averaged power of the process meaningfully, we have to take the ensemble average (D.3) of both sides of Eq. (D.7) and additionally divide both sides of Eq. (D.7) by the integration time T_i

$$\frac{1}{T_\mathrm{i}}\int_{\mathbb{R}}\langle x_{T_\mathrm{i}}(t+s)x_{T_\mathrm{i}}(t)\rangle dt = \frac{1}{2\pi}\int_{\mathbb{R}}\frac{\langle|\hat{x}_{T_\mathrm{i}}(\omega)|^2\rangle}{T_\mathrm{i}}e^{i\omega s}d\omega = \mathcal{F}^{-1}\left[\frac{\langle|\hat{x}_{T_\mathrm{i}}(\omega)|^2\rangle}{T_\mathrm{i}}\right]. \tag{D.9}$$

For $s = 0$, the right hand side of Eq. (D.9) yields the time averaged power of the stochastic process, so it does make sense to interpret

$$S_x(s, T_\mathrm{i}) \equiv \frac{\langle|\hat{x}_{T_\mathrm{i}}(\omega)|^2\rangle}{T_\mathrm{i}} \tag{D.10}$$

as power spectral density. Further, the right hand side of Eq. (D.9) can be interpreted as ensemble averaged autocorrelation function (see Eq. (D.2))

$$\Psi_x(s, T_\mathrm{i}) \equiv \frac{1}{T_\mathrm{i}}\int_{\mathbb{R}}\langle x_{T_\mathrm{i}}(t+s)x_{T_\mathrm{i}}(t)\rangle dt = \frac{1}{T_\mathrm{i}}\int_0^{T_\mathrm{i}-|s|}\langle x(t+s)x(t)\rangle dt. \tag{D.11}$$

Equation (D.9) is the Wiener-Khinchin theorem for a non-stationary stochastic processes, which states that $\Psi_x(s, T_\mathrm{i})$ and $S_x(s, T_\mathrm{i})$ form a Fourier-pair. Since for every real function x_T the corresponding PSD is an even function of frequency [10], i.e., $S_x(\omega, T_\mathrm{i}) = S_x(-\omega, T_\mathrm{i})$, the Fourier-pair can be rewritten as

$$\Psi_x(s, T_\mathrm{i}) = \frac{1}{\pi}\int_0^\infty S_x(\omega, T_\mathrm{i})\cos(\omega s)d\omega, \tag{D.12a}$$

$$S_x(\omega, T_\mathrm{i}) = 2\int_0^\infty \Psi_x(s, T_\mathrm{i})\cos(\omega s)ds. \tag{D.12b}$$

As discussed in Sect. D.2 for wide-sense stationary stochastic processes, each realization contains its full statistic information, and the limit $T_\mathrm{i} \nearrow \infty$ does exist. In this case, we can apply, instead of the ensemble average $\langle\cdot\rangle$, the limit $T \nearrow \infty$ to both sides of Eq. (D.9). We then find the Wiener-Khinchin theorem for wide-sense stationary processes [15]

$$S_x(\omega) \equiv \mathcal{F}[\Psi_x(s)], \quad \text{and} \quad \Psi_x(s) = \mathcal{F}^{-1}[S_x(\omega)], \tag{D.13}$$

where $\Psi_x(s)$ is the autocorrelation function as defined in Eq. (D.2) and the PSD is defined by

$$S_x(\omega) \equiv |\mathcal{F}[x(t)]|^2 = \lim_{T_\mathrm{i}\nearrow\infty}\frac{1}{2\pi T_\mathrm{i}}\left|\int_0^{T_\mathrm{i}} x(t)e^{-i\omega t}dt\right|^2, \tag{D.14}$$

as commonly used throughout the literature [16–18].

For the calculation of the timing jitter in Sect. 5.6, it is important to note that Eq. (D.13) permits us to calculate the variance $\mathrm{Var}(x) \equiv \langle x^2\rangle - \langle x\rangle^2$ of a real stochastic process $x(t)$ with zero mean $\langle x\rangle = 0$ from the PSD

$$\mathrm{Var}(x) = \langle x^2 \rangle = \Psi_x(0) \overset{\text{(D.12a)}}{=} \frac{1}{2\pi} \int_{\mathbb{R}} S_x(\omega) d\omega \overset{x(t)\in\mathbb{R}}{=} \frac{1}{\pi} \int_0^\infty S_x(\omega) d\omega, \quad \text{(D.15)}$$

where the second equality holds due the equivalence of covariance (D.4) and autocorrelation function (D.2) for stationary stochastic processes, in the third equality Eq. (D.12a) in the limit $T_\mathrm{i} \nearrow \infty$ has been employed, and eventually the last equality holds due to the symmetry of S_x for real $x(t)$ with zero mean ($\langle x \rangle = 0$).

D.4 Numerical Calculation of Power Spectral Density

In this section, it is briefly discussed how to obtain the PSD from numerical simulations. In numerical simulations, we obtain a finite set $\{x\} \equiv \{x_1, \ldots, x_N\}$ of samples x_n of the continuous function $x(t)$ with $x_n \equiv x(nT_s)$ and $n \in [1, \ldots, N]$, where T_s is the sampling time of the signal. We have to replace the continuous Fourier transform $\mathcal{F}$ and its inverse $\mathcal{F}^{-1}$ by a discrete-time Fourier transform F_d and its inverse, respectively,

$$F_d[\{x\}](\nu) \equiv \left\{ \frac{1}{N} \sum_{n=1}^{N} x_n e^{-i2\pi n\nu T_s} \right\}, \quad F_d^{-1}[\{\hat{x}\}](t) \equiv \left\{ \frac{1}{N} \sum_{k=1}^{N} \hat{x}_k e^{i2\pi kt\nu_s} \right\}. \quad \text{(D.16)}$$

Here, $\{\hat{x}\} \equiv \{\hat{x}_1, \ldots, \hat{x}_N\}$ is the finite set of samples of $\hat{x}$ with $\hat{x}_n \equiv \hat{x}(n\nu_s)$ and the sampling frequency $\nu_s \equiv 1/T_s$. In simulation, the system can only be integrated for finite times $T_\mathrm{i} = NT_s$. Therefore the observables, i.e., Fourier transform, power spectrum, and autocorrelation function depend on the realization of the stochastic process. Therefore, also for wide sense stationary stochastic processes, one has to average over an ensemble of $M \in \mathbb{N}$ realizations, which is denoted by $\langle \cdot \rangle_M$. The power spectrum $S_x(\nu, N)$ of $\{x\}$ is then defined as follows

$$S_x(\nu, N) \equiv T_\mathrm{i} \langle |F_d[\{x\}]|^2 \rangle_M = \frac{T_\mathrm{i}}{M} \sum_{m=1}^{M} \left| \left\{ \frac{1}{N} \sum_{n=1}^{N} x_n e^{-i2\pi n\nu T_s} \right\}_m \right|^2. \quad \text{(D.17)}$$

For non wide-sense stationary processes, $S_x(\nu, N)$ depends on the length T_i of the time-series x, i.e., on the number of samples N. For wide-sense stationary processes and T_i sufficiently large, the observables are independent of N. The factor of T_i is introduced in Eq. (D.17), because the discrete Fourier tranform of x has the dimension $[x]/\mathrm{Hz}$ [18], thus $|F_d[\{x\}]|^2$ has the dimension $[x]^2/\mathrm{Hz}^2$. The PSDs defined in Eqs. (D.10) and (D.14) have the units $[x]^2/\mathrm{Hz}$. The factor T_i ensures that the discrete PSD has the same dimension than the continuous one. Physically, it takes into account the finite resolution bandwidth $1/T_\mathrm{i}$ of the measuring instrument, i.e., of the electrical spectrum analyzer [19].

References

1. K. Lüdge, E. Schöll, Quantum-dot lasers—desynchronized nonlinear dynamics of electrons and holes. In. IEEE J. Quantum Electron. **45**(11), 1396–1403 (2009)
2. K. Lüdge, E. Schöll, Nonlinear dynamics of doped semiconductor quantum dot lasers. In. Eur. Phys. J. D **58**(1), 167–174 (2010)
3. E.J. Hinch, *Perturbation Methods. Cambridge Texts in Applied Mathematics* (Cambridge University Press, Cambridge, 1995)
4. C.M. Bender, S.A. Orszag, *Advanced Mathematical Methods for Scientists and Engineers*, Vol. 1. Springer, Berlin (2010)
5. K. Lüdge, E. Schöll, E.A. Viktorov, T. Erneux, Analytic approach to modulation properties of quantum dot lasers. In. J. Appl. Phys. **109**(9), 103112 (2011). doi:10.1063/1.3587244
6. T. Erneux, P. Glorieux, *Laser Dynamics* (Cambridge University Press, Cambridge, 2010)
7. S.H. Strogatz, *Nonlinear Dynamics and Chaos* (Westview Press, Cambridge, 1994)
8. A.M. Levine, G.H.M. van Tartwijk, D. Lenstra, T. Erneux, Diode lasers with optical feedback: stability of the maximum gain mode. Phys. Rev. A **52.5**, R3436 (1995). doi:10.1103/physreva.52.r3436 (p. 4)
9. R.L. Stratonovich, *Topics in the Theory of Random Noise*, vol. 1 (Gordon and Breach, New York, 1963)
10. C.W. Gardiner, *Handbook of Stochastic Methods for Physics, Chemistry and the Natural Sciences* (Springer, Berlin, 2002)
11. W. Horsthemke, R. Lefever, *Noise-Induced Transitions. Theory and Applications in Physics, Chemistry, and Biology* (Springer, Berlin, 1984)
12. K. Jacobs, *Stochastic Processes for Physicists: Understanding Noisy Systems* (Cambridge University Press, Cambridge, 2010). isbn: 0521765420
13. M.J. Buckingham, *Noise in Electronic Devices and Systems. Electrical and Electronic Engineering* (Wiley, New York, 1983)
14. M. Reed, B. Simon, *Functional Analysis. Methods of Modern Mathematical Physics*, vol. 1 (Academic Press, San Diego, 1980)
15. A.W Drake, *Fundamentals of Applied Probability Theory. Porbability and Statistics* (McGraw-Hill, New York, 1967)
16. J. Pomplun, *Time-delayed feedback control of noise-induced oscillations* (MA thesis, TU Berlin, 2005)
17. J. Pomplun, A.G. Balanov, E. Schöll, Long-term correlations in stochastic systems with extended time-delayed feedback. In. Phys. Rev. E **75**, 040101(R) (2007)
18. R. Paschotta, Noise of mode-locked lasers (Part I): numerical model. Appl. Phys. B: Lasers Optics **79**, 153–162 (2004). doi:10.1007/s00340-004-1547-x. issn: 0946–2171
19. B. Kolner, D. Bloom, Electrooptic sampling in GaAs integrated circuits. IEEE J. Quantum Electron. **22.1**, 79 (1986). doi:10.1109/jqe.1986.1072877.issn: 0018–9197

About the Author

Christian Otto was born in Wuppertal, Germany, in 1981. He studied physics at the University of Potsdam, at the Technische Universität Berlin, and at the Free University of Berlin. An Erasmus scholarship permitted him to study from 2004 to 2005 at the Université Joseph-Fourier in Grenoble, France. He received the Dr. rer. nat. degree from Technische Universität Berlin in 2013. His work was supervised by Prof. Dr. Eckehard Schöll, Ph.D. and Priv.-Doz. Dr. Kathy Lüdge at the Institut für Theoretische Physik. During his Ph.D. studies, he had the pleasure to spent four month in the group of Prof. Dr. Thomas Erneux at the Université Libre de Bruxelles, Belgium. His research interests include the complex nonlinear dynamics of different laser systems under delayed optical feedback and optical injection, as well as excitability and coherence resonance. He has contributed to the following publications:

- K. Lüdge, B. Lingnau, C. Otto, and E. Schöll: *Understanding electrical and optical modulation properties of semiconductor quantum-dot lasers in terms of their turn-on dynamics*, Nonlinear Phenom. Complex Syst. **15**, 350–359 (2012).
- C. Otto, K. Lüdge, A. G. Vladimirov, M. Wolfrum, and E. Schöll: *Delay induced dynamics and jitter reduction of passively mode-locked semiconductor laser subject to optical feedback*, New J. Phys. **14**, 113033 (2012).
- C. Otto, B. Globisch, K. Lüdge, E. Schöll, and T. Erneux: *Complex dynamics of semiconductor quantum dot lasers subject to delayed optical feedback*, Int. J. Bif. Chaos **22**, 1250246 (2012).

C. Otto, *Dynamics of Quantum Dot Lasers*,
Springer Theses, DOI: 10.1007/978-3-319-03786-8,

- B. Globisch, C. Otto, E. Schöll, and K. Lüdge: *Influence of carrier lifetimes on the dynamical behavior of quantum-dot lasers subject to optical feedback*, Phys. Rev. E **86**, 046201 (2012).
- J. Pausch, C. Otto, E. Tylaite, N. Majer, E. Schöll, and K. Lüdge: *Optically injected quantum dot lasers—impact of nonlinear carrier lifetimes on frequency locking dynamics*, New J. Phys. **14**, 053018 (2012).
- C. Otto, K. Lüdge, E. A. Viktorov, and T. Erneux: *Quantum dot laser tolerance to optical feedback*, in *Nonlinear Laser Dynamics—From Quantum Dots to Cryptography*, edited by K. Lüdge (WILEY-VCH, Weinheim, 2012), chapter 6, pp. 141–162.
- C. Otto, K. Lüdge, and E. Schöll: *Modeling quantum dot lasers with optical feedback: sensitivity of bifurcation scenarios*, phys. stat. sol. (b) **247**, 829–845 (2010).